Optical two-way time and frequency transfer over free space

Fabrizio R. Giorgetta*, William C. Swann, Laura C. Sinclair, Esther Baumann, Ian Coddington and Nathan R. Newbury*

The transfer of high-quality time–frequency signals between remote locations underpins many applications, including precision navigation and timing, clock-based geodesy, long-baseline interferometry, coherent radar arrays, tests of general relativity and fundamental constants, and future redefinition of the second[1-7]. However, present microwave-based time–frequency transfer[8-10] is inadequate for state-of-the-art optical clocks and oscillators[1,11-16] that have femtosecond-level timing jitter and accuracies below 1×10^{-17}. Commensurate optically based transfer methods are therefore needed. Here we demonstrate optical time–frequency transfer over free space via two-way exchange between coherent frequency combs, each phase-locked to the local optical oscillator. We achieve 1 fs timing deviation, residual instability below 1×10^{-18} at 1,000 s and systematic offsets below 4×10^{-19}, despite frequent signal fading due to atmospheric turbulence or obstructions across the 2 km link. This free-space transfer can enable terrestrial links to support clock-based geodesy. Combined with satellite-based optical communications, it provides a path towards global-scale geodesy, high-accuracy time–frequency distribution and satellite-based relativity experiments.

Fibre-optic-based time–frequency transfer can indeed support state-of-the-art optical clocks and oscillators and has been convincingly demonstrated over distances as long as 920 km (refs 17,18). However, this technique is limited to comparisons between fixed sites connected by a specialized bidirectional fibre link, but many applications instead require more flexible free-space connections between remote and possibly portable optical clocks and oscillators. In fibre-optic-based transfer, the relative clock frequencies between two laboratories are compared continuously via an optical carrier. This same basic approach could also be applied over free space[19,20] but would require a continuously operating link, which is generally incompatible with free-space transmission as turbulence will cause significant and frequent signal fading as a result of beam scintillation, beam wander and angle-of-arrival jitter[21]. Moreover, simple physical obstructions and platform motion will routinely interrupt a free-space link. Accordingly, we instead pursue the optical analogue to conventional microwave-based two-way time–frequency transfer (TWTFT). Optical TWTFT compares the elapsed time intervals between two sites rather than comparing their frequencies. Consequently, instead of a continuous link, it only requires an exchange of pulses to synchronize the sites at the start and stop times of the time interval; continuous observation between these times is unnecessary.
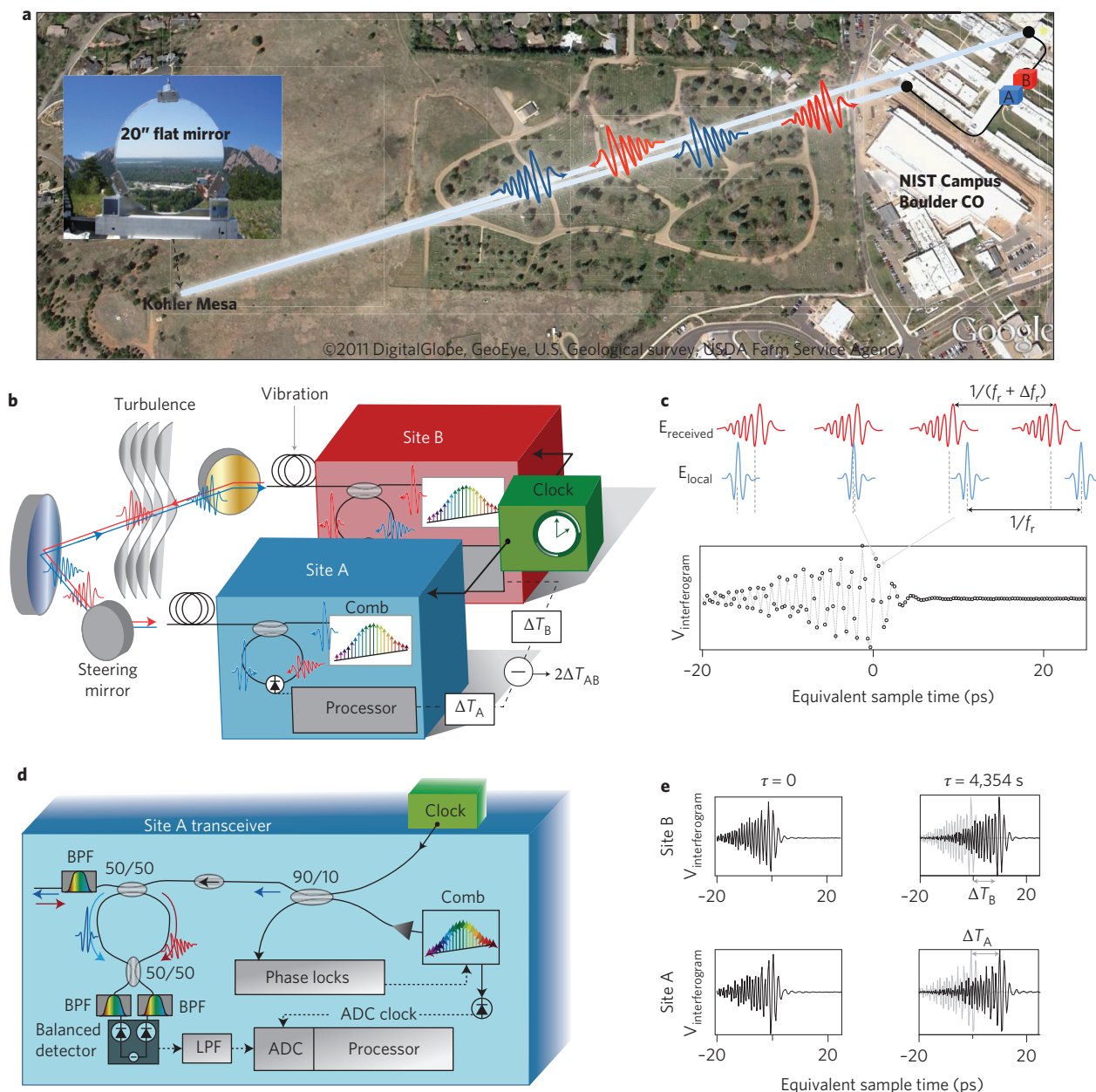
The measured time interval difference can serve diverse applications. For geodesy, two high-accuracy clocks located at different geographical locations will have a difference in time intervals that reflects their relative gravitational redshifts with a sensitivity of 1×10^{-16} per metre[1]. So, clock-based geodesy is an intriguing alternative to current time-consuming and labour-intensive levelling for geodetic calibration data[2]. Alternatively, the time interval difference can be used for jam-free synchronization of remote clocks, for synchronization of oscillators across a coherent sensor array (for example, a long-baseline interferometer or coherent radar array), or to provide position information as in conventional GPS but with much higher precision.

As required to support state-of-the-art optical clocks and oscillators, our optical TWTFT achieves residual timing deviations of 1 fs, and residual uncertainties and bias below 1×10^{-18}. Because conventional photodetection of pulse arrival times would lead to timing jitter on the level of picoseconds or worse, we implement linear optical sampling (LOS) between pulse trains of optical frequency combs[22] to obtain the femtosecond-level timing. (Balanced optical cross-correlation is a possible alternative[23,24], although it requires higher transmitted powers.) Furthermore, because the optical path-length between sites will vary due to atmospheric turbulence, platform motion and slow changes in air temperature and pressure (by 1 ppm/°C and 3 ppb/Pa at sea level), we implement a two-way exchange of pulses from frequency combs located at each site. Through the fundamental reciprocity of free-space single-mode links[25,26], this two-way exchange allows us to cancel path-length variations to within 300 nm over timescales from milliseconds to hours. Moreover, this performance is not limited by the 2 km link. As such, similar performance is expected over much longer distances.

The optical TWTFT is demonstrated over a link consisting of 2 km of free space and 500 m of optical fibre, as shown in Fig. 1. The pulse trains are transmitted over optical fibre at the cost of timing noise due to path-length variations, but with the benefit that the transceivers can be distant from the free-space launching optics[27]. To quantify the residual transfer noise, the two end sites A and B are adjacent and use a common optical oscillator. In all other regards, the two sites are independent. At each site, a coherent pulse train (comb) is generated by phase-locking a femtosecond fibre laser to the optical oscillator but with the repetition rates differing by Δf_r between sites. As with other dual-comb applications[22], LOS between these mismatched optical pulse trains gives time and phase information about the underlying optical waveform over broad optical bandwidths (1 THz) as a train of interferograms (cross-correlations). Ideally, these interferograms repeat at $\tau_0 = 1/\Delta f_r$ so that the 0th and nth interferograms are separated by exactly $\tau = n\tau_0$. However, timing differences or path-length variations between the sites will cause an additional time offset between the 0th and nth interferograms of

$$\Delta T_A(\tau) = \Delta T_{Path}(\tau) + \Delta T_{AB}(\tau)$$

National Institute of Standards and Technology, 325 Broadway, Boulder, Colorado 80305, USA. *e-mail: fabrizio@nist.gov; nnewbury@boulder.nist.gov

Figure 1 | Optical two-way time–frequency transfer. a, Transfer takes place between two co-located sites A and B sharing a common optical oscillator or 'clock', allowing evaluation of the residual timing deviation. The sites are linked by 385 m and 115 m optical fibre paths (black lines) from the laboratory to each free-space launch for the 2 km air path (grey line). **b**, A comb, consisting of a femtosecond fibre laser phase-locked to the common clock, generates a pulse train that is coherent (that is, 'ticks' synchronously) with the clock at a repetition rate of $f_r \approx 100$ MHz for Site A and $f_r + \Delta f_r \approx 100.003$ MHz for Site B. These pulse trains are exchanged between sites. **c**, LOS detects the arrival of the received pulses in analogy with sampling oscilloscopes. The local comb pulse train (blue) optically samples the received comb pulses (red) at varying delays to generate an interferogram (black trace, measured data) with an equivalent time step of $\sim \Delta f_r / f_r^2$ per point. **d**, The set-up is implemented using commercial fibre-optic components. The comb output is amplified (grey triangle) and bandpass-filtered (BPF) to 0.9 THz (7 nm) to generate an ~ 4 mW pulse train near 193 THz. The superposed received and local comb pulses are detected, low-pass filtered (LPF), digitized with an analogue-to-digital converter (ADC), and the resulting interferogram processed to find $\Delta T_{A(B)}$ (see Methods and Supplementary Discussion). **e**, Measured interferograms (black) at $\tau = 0$ and 4,354 s (1.2 h). The grey traces indicate the interferogram expected in the absence of path length or timing variations. For the case shown, the one-way delay increased by 11 ps (3.3 mm) in 1.2 h.

and

$$\Delta T_B(\tau) = \Delta T_{Path}(\tau) - \Delta T_{AB}(\tau)$$

for sites A and B, respectively, where ΔT_{Path} is the cumulative change in the one-way time-of-flight between sites (assumed identical for each direction because of the reciprocity of single-mode

links[25,26]), and ΔT_{AB}, the quantity of interest, is the cumulative timing difference between the clock and oscillator at site A and site B. Both ΔT_{Path} and ΔT_{AB} are assumed to vary slowly over τ_0. The two-way time difference is $\Delta T_{AB} = (\Delta T_A - \Delta T_B)/2$. Note that measurements at only $n = 0$ and $n = N$ are sufficient to find $\Delta T_{AB}(\tau)$, provided the combs remain continuously phase-locked to the optical oscillator.
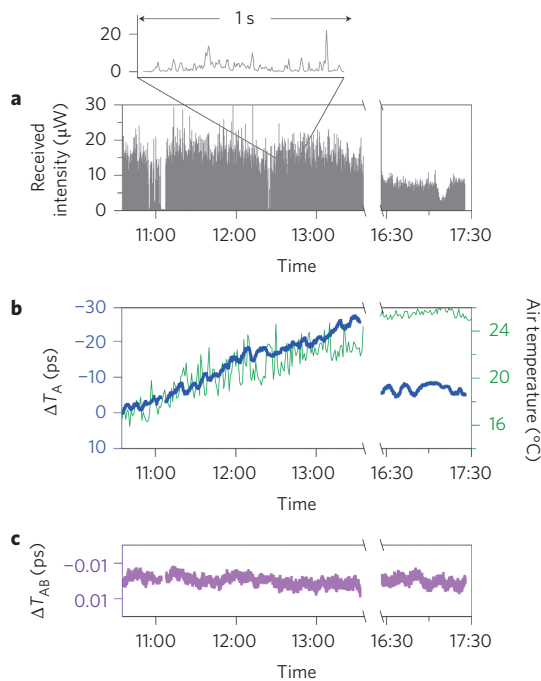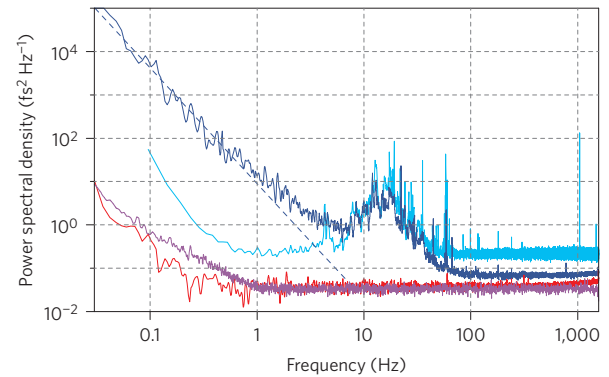
Figure 2 | Example data. a, The detected intensity at site A exhibits the strong fluctuations and fading characteristic of coherent links over turbulent paths. **b**, Variation in the one-way time-of-flight ΔT_A (blue, left axis) and air temperature (green, right axis). The reset in ΔT_A at 13:45 is a consequence of a phase slip between the clock and one comb. **c**, Residual timing difference ΔT_{AB} acquired at $\tau_0 = 300$ μs intervals and averaged over 100 ms time intervals. The slow ripple (standard deviation of 2.5 fs) is attributed to temperature-induced path-length fluctuations within the transceiver and not the reciprocal free-space link.

Figure 3 | Power spectral densities. The PSD for the time-of-flight $S_A(f)$ across 2 km of air and 500 m of optical fibre (dark blue line) has contributions from the 500 m optical fibre (light blue line) at intermediate frequencies and the atmospheric piston effect $S_P(f)$ (dashed blue line) at low frequencies, calculated for 1 m s^{-1} wind speed and $C_n^2 = 2.5 \times 10^{-14}$ m$^{-2/3}$. In contrast, the PSD for the two-way timing difference $S_{AB}(f)$ (dark purple line) has negligible contribution from atmospheric turbulence or fibre noise and lies directly on top of the two-way PSD measured over a shorted path (red line).

The interpretation of $\Delta T_{AB}(\tau)$ is straightforward: a linear fit yields a slope that is exactly the fractional offset in time or in frequency, given by $\Delta f_{Clock}/f_{Clock}$, where Δf_{Clock} is the frequency difference between the clocks at the sites, with nominal frequency f_{Clock}. Here we use a common 'clock' so that the fractional offset should be zero in the absence of systematic bias. The Allan deviation of $\Delta T_{AB}(\tau)$ expresses the uncertainty on the measured fractional offset.

Figure 2 shows data from one day. The effects of turbulence are evident. Based on the measured angle-of-arrival jitter[21], the turbulence structure constant is within the range $C_n^2 \approx 1 \times 10^{-15}$ to 1×10^{-14} m$^{-2/3}$. This angular jitter is mainly cancelled via feedback to a steering mirror, but the link is still interrupted because of turbulence-induced scintillation, physical obstructions or loss of steering-mirror tracking. For example, from 12:00 to 13:00, interruptions occurred 23% of the time, with durations up to 10 s, while from 16:30 to 17:30, they occurred 0.3% of the time, with durations up to 0.5 s. (During processing, an interruption corresponds to the received signal fading below 20 nW at the photodiode, or ~1,500 photons per pulse.) Both ΔT_A and ΔT_B, and therefore ΔT_{AB}, are tracked through the interruptions, because the combs remain phase-locked to the underlying clock. However, a slip of the phase lock of a comb resets the measurement, as at 13:35, in practice limiting the measurement periods to a few hours. A zero-dead-time counter, more robust phase locks or possibly real-time processing[28] could suppress this problem.

Figure 3 presents timing-jitter power spectral densities (PSD) $(S_A(f))$ of the one-way time difference ΔT_A and $(S_{AB}(f))$ of the two-way time difference ΔT_{AB}. The different contributions to the one-way noise, $S_A(f)$, can be deconstructed. Above 100 Hz, the noise floor is attributed to detector noise, shot noise and

phase jitter on the combs' phase lock to the common clock. Between 20 Hz and 100 Hz, $S_A(f)$ is dominated by vibration-induced fibre noise. (Even at shorter fibre lengths, platform vibrations induce similar noise through the motion of the free-space launching optics[29].) Below 20 Hz, the turbulence-induced atmospheric piston effect dominates, with the contribution $S_P(f) = 0.016 c^{-2} C_n^2 L V^{5/3} f^{-8/3}$ s^2 Hz^{-1} over $V/L_0 < f < 0.3V/D$, where $L \approx 2$ km is the link length, $V \approx 1$ m s^{-1} is the wind speed, c is the speed of light, $L_0 \approx 100$ m is the outer scale and $D \approx 5$ cm is the aperture diameter[21,30]. In stark contrast to $S_A(f)$, the PSD of the two-way time difference $S_{AB}(f)$ follows the transceiver noise, which is 10^3 to 10^4 times lower than $S_A(f)$.

As shown in Fig. 4, the residual modified Allan deviation for ΔT_{AB} falls below 1×10^{-18} around a measurement interval of 1,000 s. Moreover, it equals the Allan deviation for a shorted link, indicating that transceiver noise, and not residual free-space path-length variations, limits performance. Even if the measurement is restricted to two 100 ms intervals at the start and stop of the overall interval, the resulting instability (equivalent to the over-lapping Allan deviation for 100 ms smoothed data) still reaches 1×10^{-18} at a few thousand seconds. The corresponding timing deviation, shown in Fig. 4b, averages down as $\sqrt{\tau}$ until 1 s and then reaches a floor, which reflects the ~1/f increase in $S_{AB}(f)$ for $f < 1$ Hz. We attribute this non-white phase noise to drifts in non-common fibre path lengths within the transceivers (Supplementary Fig. S1).

The instability (Allan deviation) is one measure of performance, but it is equally important that the transfer introduces no frequency offsets, that is, non-zero slope to ΔT_{AB}. As shown in Fig. 4c, the bias, or fractional offset, is below ~4×10^{-19} (1σ) for the two-way measurement. In contrast, one-way transfer (ΔT_A) can exhibit a significant offset. For example, a linear 10 °C h^{-1} temperature increase over 2 km results in a 1.4×10^{-14} offset, much larger than the Allan deviation, and launch-platform motion would lead to even higher offsets via Doppler shifts.

The current demonstration covers 2 km but is not distance-limited, so equivalent performance out to much longer terrestrial links should be possible. Very long-distance or global coverage will require ground-to-satellite or satellite-to-satellite optical TWTFT, and could replace conventional or future microwave-based approaches[8–10] for high-performance applications. Although
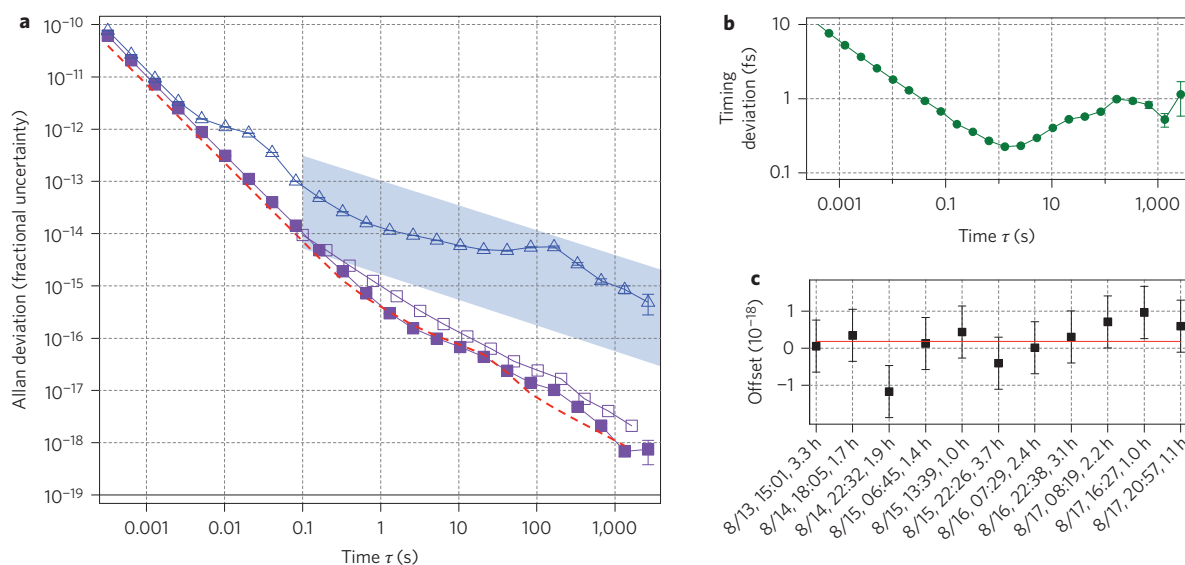
Figure 4 | Precision (residual Allan deviation) and offset of the optical TWTFT, evaluated over multiple data sets covering 24 h of acquisition.
a, Residual modified Allan deviation M_{DEV} for optical TWTFT (solid squares), calculated from ΔT_{AB}, is well below the instabilities of state-of-the-art optical clocks (shaded region)[1,11–15,17] and lies directly on the modified Allan deviation for a shorted path (red dashed line). The overlapping Allan deviation at 100 ms averaging (open squares) corresponds to two isolated 100 ms measurements at the start and end of the time interval and exhibits similar performance. In contrast, the modified Allan deviation for one-way transfer (open triangles), calculated from ΔT_A, is significantly higher and limited by path-length fluctuations. **b**, Timing deviation $T_{DEV} = (\tau/\sqrt{3})M_{DEV}$ of optical TWTFT. **c**, The fractional offset, or bias, across 11 data sets (squares labelled by start time and duration) has a weighted average (solid line) of $1.8 \times 10^{-19} \pm 2.1 \times 10^{-19}$, consistent with zero as expected for the common clock (and well below the accuracy of the best optical clocks). The uncertainty per point is estimated at 7×10^{-19} assuming a flat Allan deviation at integration times beyond 2,000 s.

the integrated turbulence from ground to satellite is similar to that across this 2 km link, additional issues arise in satellite-based optical TWTFT. For example, longer delays tax the reciprocity condition; large Doppler shifts and platform displacements must be handled; and a coherent link must be maintained, even if intermittently. Fortunately, satellite-based optical communications is an active area of development[21,26,31]. The optical TWTFT demonstrated here is compatible with these advancements, and a marriage of the two could usher in new possibilities in ultraprecise and accurate global time–frequency distribution, global geodesy and satellite-based experiments on general relativity.

Methods

The experimental set-up at each site followed previous comb-based ranging arrangements[22] (Supplementary Figs S1, S2). The surrogate common optical clock was realized by a pair of continuous-wave (c.w.) fibre lasers at 192.1 THz and 195.3 THz, which were separated by ~3.2 THz and phase-locked to the same high-finesse ($F \approx 180,000$) optical cavity. The two 100 MHz femtosecond erbium-fibre lasers were phase-locked with identical radiofrequency offsets to this pair of lasers, but such that one comb had 31,846 teeth and one had 31,847 teeth spanning the 3.2 THz, yielding a repetition rate difference of $\Delta f_r \approx 3$ kHz. The phase noise on the four phase locks, integrated from 10 Hz to 10 kHz, was below 1 rad.

Relative timing jitter due to phase-lock noise is indistinguishable from a clock time-base difference and is therefore included in ΔT_{AB}. Carrier-frequency noise combined with differential chirp between the two combs causes excess measured timing jitter. We therefore compensated the dispersion of the 350 m of single-mode fibre with 150 m of dispersion-compensating fibre (DCF). (This effect is illustrated by the elevated white noise floor of the fibre-noise PSD, shown as the light blue trace in Fig. 3, which was acquired without DCF.)

The interferograms between the pulse trains were detected with a commercial 100 MHz balanced detector, low-pass-filtered at 50 MHz, and digitized at 12 bits synchronously with the local comb's repetition rate. The 512 samples across the centreburst of the interferograms were saved, together with the received intensity and steering-mirror correction signals.

Signal processing of the interferograms was accomplished in the spectral domain (Supplementary Discussion.) Each interferogram acquired at time τ was Fourier-transformed with respect to equivalent time to determine its spectral phase $\theta(\nu, \tau)$ versus optical frequency ν. An interferogram near the start served as the reference,

$\theta(\nu, 0)$. The slope of the difference, $\theta(\nu, \tau) - \theta(\nu, 0)$, is equal to $+2\pi\Delta T_A(\tau)$ (or $-2\pi\Delta T_B(\tau)$). The slope is only extracted if the signal-to-noise ratio is sufficient to guarantee correct phase unwrapping of $\theta(\nu, \tau)$.

References

1. Chou, C. W., Hume, D. B., Rosenband, T. & Wineland, D. J. Optical clocks and relativity. *Science* **329**, 1630–1633 (2010).
2. Bondarescu, R. *et al.* Geophysical applicability of atomic clocks: direct continental geoid mapping. *Geophys. J. Int.* **191**, 78–82 (2012).
3. Müller, J., Soffel, M. & Klioner, S. Geodesy and relativity. *J. Geod.* **82**, 133–145 (2008).
4. Schiller, S. *et al.* Einstein gravity explorer—a medium-class fundamental physics mission. *Exp. Astron.* **23**, 573–610 (2009).
5. Wolf, P. *et al.* Quantum physics exploring gravity in the outer solar system: the SAGAS project. *Exp. Astron.* **23**, 651–687 (2009).
6. Uzan, J. The fundamental constants and their variation: observational and theoretical status. *Rev. Mod. Phys.* **75**, 403–455 (2003).
7. Gill, P. When should we change the definition of the second? *Phil. Trans. R. Soc. A* **369**, 4109–4130 (2011).
8. Bauch, A. *et al.* Comparison between frequency standards in Europe and the USA at the 10^{-15} uncertainty level. *Metrologia* **43**, 109–120 (2006).
9. Samain, E. *et al.* The T2L2 ground experiment time transfer in the picosecond range over a few kilometres. *Proceedings of the 20th European Frequency and Time Forum* 538–544 (2006).
10. Cacciapuoti, L. & Salomon, C. Space clocks and fundamental tests: the ACES experiment. *Eur. Phys. J. Special Topics* **172**, 57–68 (2009).
11. Chou, C. W., Hume, D. B., Koelemeij, J. C. J., Wineland, D. J. & Rosenband, T. Frequency comparison of two high-accuracy Al^+ optical clocks. *Phys. Rev. Lett.* **104**, 070802 (2010).
12. Katori, H. Optical lattice clocks and quantum metrology. *Nature Photon.* **5**, 203–210 (2011).
13. Ludlow, A. D. *et al.* Sr lattice clock at 1×10^{-16} fractional uncertainty by remote optical evaluation with a Ca clock. *Science* **319**, 1805–1808 (2008).
14. Fortier, T. M. *et al.* Generation of ultrastable microwaves via optical frequency division. *Nature Photon.* **5**, 425–429 (2011).
15. Jiang, Y. Y. *et al.* Making optical atomic clocks more stable with 10^{-16}-level laser stabilization. *Nature Photon.* **5**, 158–161 (2011).

16. Yamaguchi, A. *et al.* Direct comparison of distant optical lattice clocks at the 10^{-16} uncertainty. *Appl. Phys. Express* **4,** 082203 (2011).
17. Predehl, K. *et al.* A 920-kilometer optical fiber link for frequency metrology at the 19th decimal place. *Science* **336,** 441–444 (2012).
18. Lopez, O. *et al.* Simultaneous remote transfer of accurate timing and optical frequency over a public fiber network. *Appl. Phys. B* **110,** 3–6 (2013).
19. Sprenger, B., Zhang, J., Lu, Z. H. & Wang, L. J. Atmospheric transfer of optical and radio frequency clock signals. *Opt. Lett.* **34,** 965–967 (2009).
20. Djerroud, K. *et al.* Coherent optical link through the turbulent atmosphere. *Opt. Lett.* **35,** 1479–1481 (2010).
21. Andrews, L. C. & Phillips, R. L. *Laser Beam Propagation through Random Media* (SPIE Press, 1998).
22. Coddington, I., Swann, W. C., Nenadovic, L. & Newbury, N. R. Rapid and precise absolute distance measurements at long range. *Nature Photon.* **3,** 351–356 (2009).
23. Kim, J., Cox, J. A., Chen, J. & Kärtner, F. X. Drift-free femtosecond timing synchronization of remote optical and microwave sources. *Nature Photon.* **2,** 733–736 (2008).
24. Lee, J., Kim, Y. J., Lee, K., Lee, S. & Kim, S. W. Time-of-flight measurement with femtosecond light pulses. *Nature Photon.* **4,** 716–720 (2010).
25. Shapiro, J. H. Reciprocity of the turbulent atmosphere. *J. Opt. Soc. Am.* **61,** 492–495 (1971).
26. Parenti, R. R., Michael, S., Roth, J. M. & Yarnall, T. M. Comparisons of C_n^2 measurements and power-in-fiber data from two long-path free-space optical communication experiments. *Proc. SPIE* **7814,** 78140Z (2010).
27. Marra, G. *et al.* High-resolution microwave frequency transfer over an 86-km-long optical fiber network using a mode-locked laser. *Opt. Lett.* **36,** 511–513 (2011).
28. Roy, J., Deschênes, J-D., Potvin, S. & Genest, J. Continuous real-time correction and averaging for frequency comb interferometry. *Opt. Express* **20,** 21932–21939 (2012).
29. Giorgetta, F. R. *et al.* in *CLEO: Applications and Technology* CTh5D.10 (Optical Society of America, 2012).
30. Conan, J., Rousset, G. & Madec, P-Y. Wave-front temporal spectra in high-resolution imaging through turbulence. *J. Opt. Soc. Am. A* **12,** 1559–1570 (1995).
31. Koishi, Y. *et al.* in *International Conference on Space Optical Systems and Applications (ICSOS)* 88–92 (IEEE, 2011).

Competing financial interests
The authors declare no competing financial interests.